Supporting Information

X-ray Structures of Human Furin in Complex with Competitive Inhibitors

Sven O. Dahms[1], Kornelia Hardes[2], Gero L. Becker[2],Torsten Steinmetzer[2], Hans Brandstetter[3], Manuel E. Than[1]*

[1] Protein Crystallography Group, Leibniz Institute for Age Research - Fritz Lipmann Institute (FLI), Beutenbergstr. 11, 07745 Jena, Germany

[2] Department of Pharmaceutical Chemistry, Philipps University Marburg, Marbacher Weg 6, D-35032 Marburg, Germany

[3] Department of Molecular Biology, University of Salzburg, Billrothstrasse 11, A-5020 Salzburg, Austria

* Corresponding author e-mail address: than@fli-leibniz.de

Table of contents

	Page
Supplementary Methods	S1-S5
Supplementary Figures	
Supplementary Figure 1	S6
Supplementary Figure 2	S7
Supplementary Figure 3	S8-9
Supplementary Figure 4	S10
Supplementary Figure 5	S11
Supplementary Tables	
Supplementary Table 1	S12
Supplementary Table 2	S12
Supplementary References	S13-S14

Supplementary Methods

Expression in HEK293S-cells

For protein expression the coding sequence of human pro-Furin, covering the amino acids 23-574, was inserted into the plasmid pHLsec [1]. Using the restriction sites XhoI and AgeI, the insert was placed upstream to a secretion signal sequence encoded by the expression vector. The native protein sequence was modified with a Factor-Xa cleavage site and a His-tag, resulting in the artificial C-terminus SGSLVPRGSHHHHHH that is expressed after Ala574.

Homogenously glycosylated protein was produced by transient transfection of a HEK293 Gnt^- cell line [2], using PEI as transfection reagent. Transfection and expression was performed according to the procedure described by Aricescu and coworkers [1]. The ratio (w/w) of transfection reagent to plasmid-DNA was 2:1 and 0.5 µg DNA were used per cm^2 of cultured cells. Addition of 10 mM $CaCl_2$ increased the expression yield and transfection was carried out at approx. 75% confluence of the culture. Multi-layer flasks (Triple-Flask, Nunc) were used for large scale protein production. The medium was harvested 72 h and 120 h post transfection. 120 ml and 60 ml medium were used during the first and second culture period, respectively. Typically 2-4 mg of recombinant human furin were obtained per liter conditioned medium.

Purification

For storage the conditioned medium was centrifuged (20 min, 4500 g, 20°C) and frozen in liquid nitrogen. Prior to purification the medium was thawed in a water bath at 25°C and filtrated, using a PVDF membrane (0.45 µm pore size, Merck-Millipore). Next, dialysis was

performed for 16 h at 20°C against a 20-fold excess of 25 mM Tris, pH 8.0, 250 mM NaCl, 5 mM $CaCl_2$ with NADIR (cutoff 10-20 kDa, Carl Roth GmbH) dialysis membrane. Human furin was purified in a three-step chromatography scheme, using an Aekta Explorer FPLC system (Amersham Pharmacia Biotech). Before application to a 1 ml HisTrap FF Crude (GE-Healthcare) affinity column Imidazol was added to the medium, achieving an end concentration of 10 mM. The column was washed with 10 column volumes of buffer A (100 mM Tris, pH 8.0, 500 mM NaCl, 5 mM $CaCl_2$) supplemented with 10 mM imidazole and 10 column volumes of buffer A supplemented with 20 mM imidazole. The protein was eluted with 500 mM imidazol in buffer A. The eluate was diluted 10-fold in buffer B (10 mM Hepes, pH 7.5, 100 mM NaCl, 2 mM $CaCl_2$) and further purified by inhibitor based affinity chromatography. The inhibitor affinity column was prepared by immobilization of a biotinylated inhibitor on a HiTrap Strepavidin HP column as described previously [3]. The inhibitor column was washed with 10 column volumes of buffer B and the protein was eluted with buffer B supplemented with 500 mM NaCl. The eluate was concentrated to 2 mg ml^{-1}, using an Amicon ultrafiltration membrane with 30 kDa cutoff (Merck-Millipore). The sample was applied to a S 200 10-300 GL gel permeation chromatography column (GPC, GE-Healthcare) and separated at 0.5 ml min^{-1} in buffer B. The enrichment of the protein was monitored after each purification step by determination of the specific activity and by SDS-PAGE analysis (Supplementary Figure 1). Typically 50% of the starting material used was recovered as purified sample by the described preparation scheme.

Enzyme kinetics

Furin activity assays were performed in 96-well plates at 37°C in a fluorometer (POLARstar Galaxy, BMG Labtech) using 380 nm as the excitation and 460 nm as the emission wavelength as described previously [4]. The assay buffer contained 100 mM Hepes, pH 7.0,

5 mM $CaCl_2$, 0.5% (v/v) TritonX-100 at 37°C and 200 µM of the substrate pGlu-Arg-Thr-Lys-Arg-AMC (Bachem).

The inhibition constant of Phac-RVR-Amba was determined at room temperature according to the method of Dixon [5], using the fluorescence plate reader Safire2 (Tecan) at 380 nm and 460 nm as excitation and emission wavelengths, respectively. Pyr-Arg-Thr-Lys-Arg-AMC was used as substrate in 100 mM HEPES buffer, pH 7.0, containing 0.2% (v/v) Triton X-100, 2 mM CaCl2, 0.02% sodium azide and 1 mg ml^{-1} BSA, as described previously [6]. The lowest inhibitor concentration used was at least 10 times higher than the enzyme concentration in the assay to avoid tight binding conditions.

The steady rates calculated from the linear progress curves obtained in presence of various concentrations (10 nM-0.59 nM in the assay) of the tight binding inhibitors ortho-, meta- or para-Phac-RVR-Amba and of a constant substrate concentration (Pyr-Arg-Thr-Lys-Arg-AMC, 12.5 µM in the assay) were fitted to equation 1 [7], where v_0 is the constant velocity in absence of inhibitor, I and E are the inhibitor and enzyme concentrations, and Ki* is an apparent inhibition constant at the substrate concentration used.

(1) $$v = v_0 \cdot \frac{\left[\left(K_{i^*}+I-E\right)^2+4K_{i^*}\cdot E\right]^{\frac{1}{2}}-\left(K_{i^*}+I-E\right)}{2\cdot E}$$

The true Ki values were calculated from these apparent inhibition constants using equation 2.

(2) $$K_i = \frac{K_{i^*}}{1+\left(\frac{S}{K_m}\right)}$$

All kinetic measurements were performed in triplicates.

Crystallization and Structure Determination

Furin was concentrated to 140-150 µM (7.5 mg ml^{-1}) and I1 [8] was added to a final concentration of 290 µM prior to crystallization. 15 initial conditions were identified in the Hampton crystal screens I+II (Hampton Research). The most promising crystals grew in 4 M sodium formate and were optimized in several fine- and additive screens. Final crystals were grown within two weeks up to a size of 40×80×1000 µm at 30°C in 50 mM Tris, pH 8.5, 2.8 M sodium formate and 0.015 mM Cymal-7 as additive. For the structural investigation of the complex of Furin with I2 [6] I1-containing crystals were washed 5× in 0.5 µl crystallization solution supplemented with 3 mM of the inhibitor I2 and finally incubated for 5 days. Before data collection the rod shaped crystals were fragmented into approx. 250 µm sized parts and mounted in 50×500 µm elliptical loops (Molecular Dimensions) for diffraction data collection at 100 K at the BESSY-II beamline 14.1 of the Helmholtz-Zentrum Berlin (HZB) [9]. Flash cooling was performed in crystallization solution, supplemented with 15% (v/v) ethylenglycol. For correct identification of additional metal ions observed in the structure a second dataset was collected from another section of the same I1-crystal at low energy. XDS (v.03/2013 [10]) was used for integration and data reduction and the data were analyzed with programs of the CCP4-suite (CCP4 v.6.3.0, CCP4 interface v.2.2.0, [11]). The R_{free} sets of reflections were defined in thin shells, using DATAMAN [12]. The structure was solved by molecular replacement, using the structure of mouse Furin (PDB-ID 1P8J, [13]) as search model in PHASER [14]. The crystals belong to the spacegroup $P2_12_12_1$ with 6 furin molecules in the asymmetric unit, each with one inhibitor molecule bound to the active site cleft. Model building was carried out in COOT (v.0.6.2, [15]). CNS (v.1.3, [16]) was used for refinement, applying tight NCS-restraints to the main chain atoms of the protein. Refinement parameters of the meta-guanidinomethyl-Phac-, Phac- and Amba-moieties of the inhibitors, including bond length, bond angels, dihedrals and force constants, were derived from small molecule

structures of the Cambridge structural database [17]. B-factor analysis was performed with MOLEMAN [18]. PYMOL (http://www.pymol.org) was used for molecular graphics.

Thermal denaturation assays

Thermal denaturation analysis (also called thermoflour assay, [19]) was performed in 40 mM sodium borate, pH 7.5, 100 mM NaCl, 2 mM NaCl, 2 mM $CaCl_2$ and 15x Sypro-Orange (Life Technologies), adding 1.5 µM of each, the protease and the inhibitor. The borate buffer was chosen because of its pH-stability in the desired temperature interval and because phosphate buffer would precipitate $CaCl_2$, affecting the substrate binding properties and the heat stability of Furin. Melting curves were determined with an IQ5 realtime PCR cycler (Biorad), measuring the increase of the fluorescence at excitation and emission wavelengths of 490 nm and 575 nm, respectively. Heating was performed in 0.2°C steps with a subsequent dwell time of 10 s. The first order derivatives of the data were determined in SPECTRA ANALYSIS (v.1.53.04, Jasco Corporation) using the Savitzky-Golay method. The melting temperatures (T_m) were derived from the peak temperatures of the first order derivatives of the melting curves.

Supplementary Figures

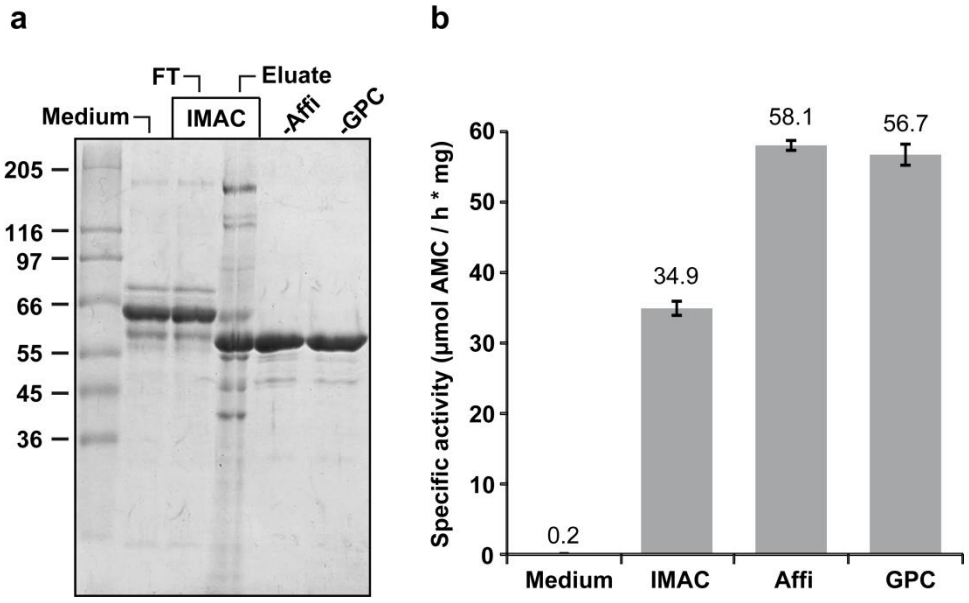

Supplementary Figure 1 Purification of human furin. (a) SDS page analysis of samples obtained during purification of conditioned medium collected from HEK293S cells (Medium), flow-through (FT) and eluate of immobilized metal ion affinity chromatography (IMAC), eluate after inhibitor based affinity purification (Affi) and eluate after gel permeation chromatography (GPC). (b) Specific activity of human furin in the conditioned medium, after IMAC, Affi and GPC.

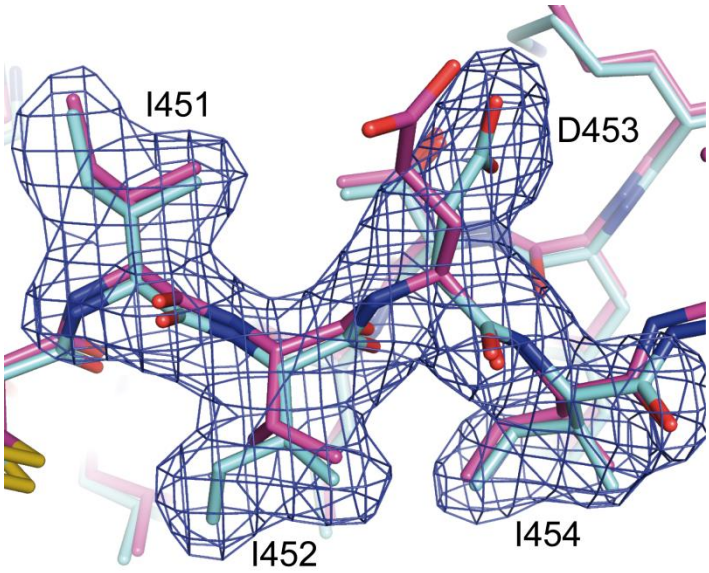

Supplementary Figure 2 Single amino acid substitutions between human and mouse furin. Human (cyan) and mouse (magenta) furin were aligned and are shown as stick model. The $\boldsymbol{F}_o$-$\boldsymbol{F}_c$ difference electron density omit map is contoured at 3.5 σ for the amino acids Ile451-Ile454 (human furin sequence).

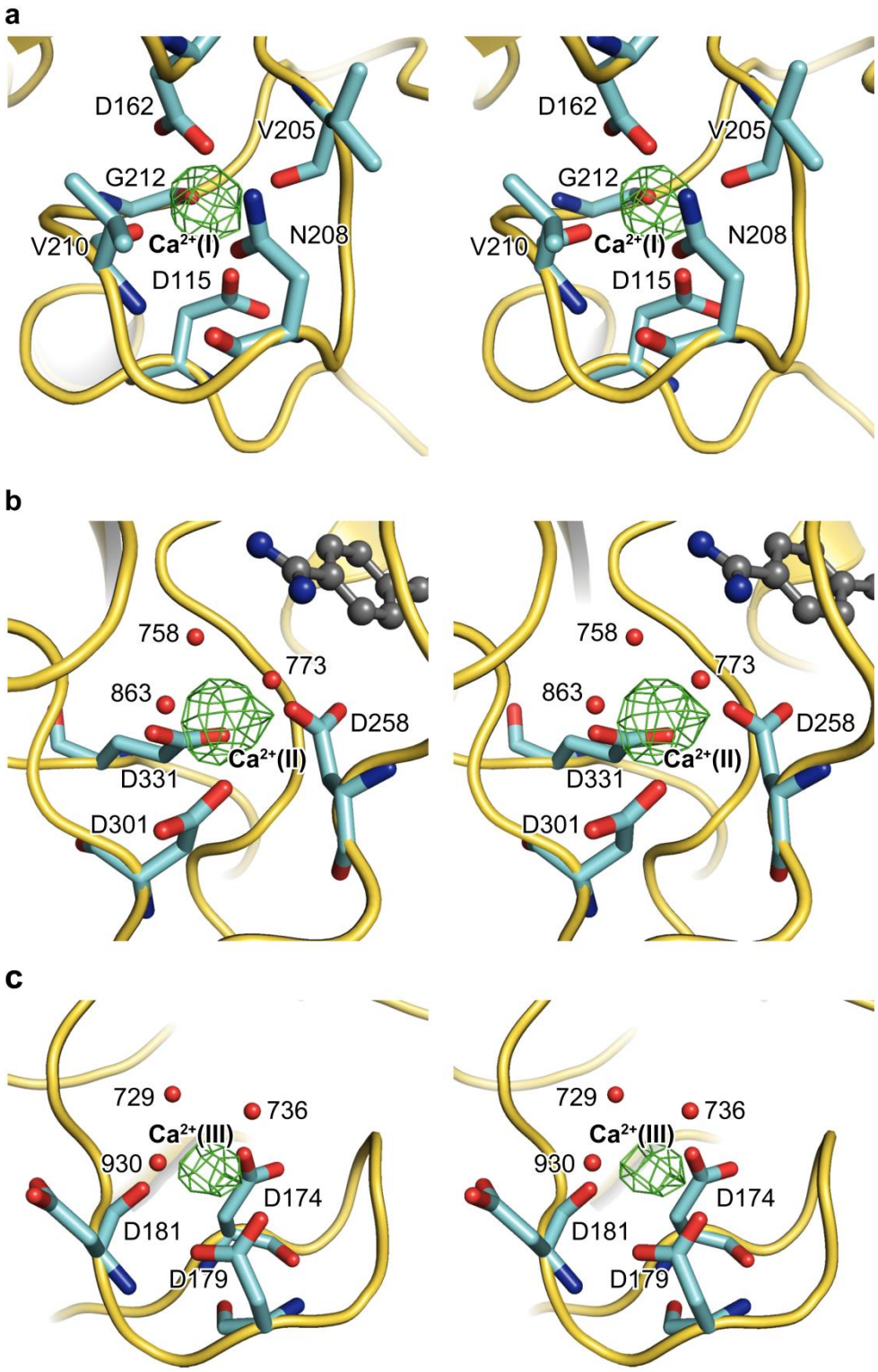

Supplementary Figure 3 Detailed view on the calcium binding sites observed in the human furin structure. The stereo panels show the Cα-carbon trace of the protease as cartoon

representation (yellow). The inhibitor and important residues of furin are shown in dark grey (ball and stick model) and in cyan (stick model), respectively. Using data measured at a wavelength of 2.07 Å (Supplementary Table 2) and phases from the refined model (Ca^{2+}-ions were omitted), an anomalous difference map was calculated (green mesh, contoured at 5 σ), indicating the location of potential calcium ions. Selected water molecules are shown as red spheres. (a) Calcium binding site 1 (Ca^{2+} I). (b) Calcium binding site 2 (Ca^{2+} II). (c) Calcium binding site 3 (Ca^{2+} III).

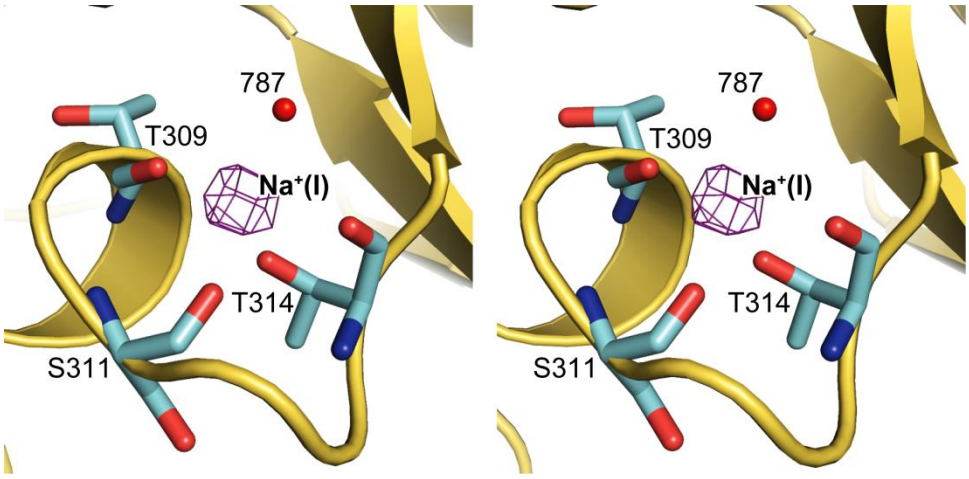

Supplementary Figure 4 Detailed view on the sodium binding site observed in the human furin structure. The stereo panel shows the Cα-carbon trace of the protease as cartoon representation (yellow). The $\boldsymbol{F}_o$-$\boldsymbol{F}_c$ difference electron density omit map of the sodium ion, Na^+ (I), is shown as purple mesh and is contoured at 10 σ. Selected water molecules are shown as red spheres.

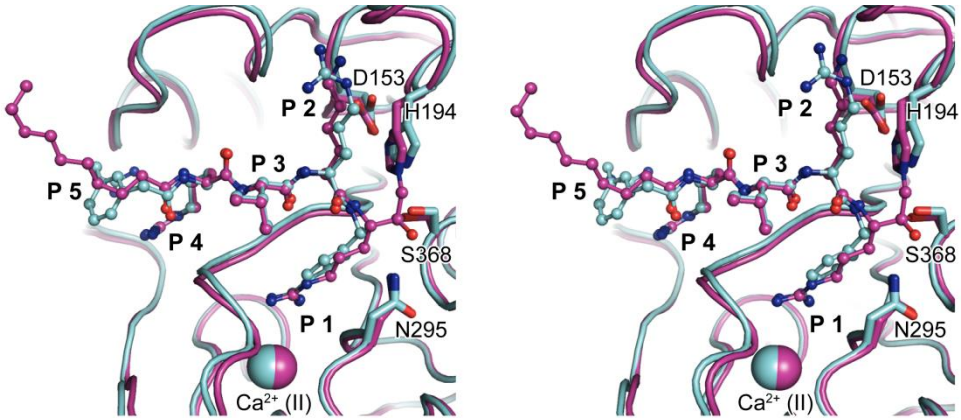

Supplementary Figure 5 Comparison of the inhibitor bound active site clefts of human and mouse furin. Human and mouse furin are colored cyan and magenta, respectively. The protein backbone of the aligned structures is shown in ribbon representation. The side chains of the catalytic residues are given as stick model. Inhibitor I1 (human furin) and the covalently attached dec-Arg-Val-Lys-Arg-chloromethylketone peptide (mouse furin) are shown as ball and stick model. Ca2 is shown as sphere.

Supplementary Tables

Supplementary Table 1 Inhibitor constants.

Inhibitor	Ki (pM)	
	CHO-expressed furin with complex glycosylation [a]	HEK293S-expressed furin with homogenous glycosylation (this study)
Phac-RVR-Amba (I2)	810	977 ± 196
ortho-guanidinomethyl- Phac-RVR-Amba	291	196 ± 15.2
meta-guanidinomethyl- Phac-RVR-Amba (I1)	8	16.7 ± 0.6
para-guanidinomethyl- Phac-RVR-Amba	16	9.7 ± 1.5

[a] Values taken from: refs 6 and 8

Supplementary Table S2 Data collection statistics of anomalous data.

Inhibitor	I1
Wavelength (Å) / energy (keV) of data collection	2.07 / 6
Unit cell parameters	$P2_12_12_1$
a (Å), b (Å), c (Å)	141.97, 152.78, 167.90
Resolution range [a] (Å)	50.0-2.5 (2.65-2.50)
Rpim [a, b] (%)	7.1 (38.8)
Rmeas [a] (%)	9.7 (54.2)
I/sigI [a]	9.6 (1.9)
Anomalous completeness [a] (%)	93.9 (89.0)
Anomalous observations: total / unique	442,572/ 227,804

[a] Highest resolution shell is given in parentheses.

[b] Calculated in SCALA[20] in the resolution ranges (given in Å): 50-2.51(2.64-2.51).

Supplementary References

[1] Aricescu, A. R., Lu, W., and Jones, E. Y. (2006) A time- and cost-efficient system for high-level protein production in mammalian cells, *Acta crystallographica 62*, 1243-1250.

[2] Reeves, P. J., Callewaert, N., Contreras, R., and Khorana, H. G. (2002) Structure and function in rhodopsin: high-level expression of rhodopsin with restricted and homogeneous N-glycosylation by a tetracycline-inducible N-acetylglucosaminyltransferase I-negative HEK293S stable mammalian cell line, *Proceedings of the National Academy of Sciences of the United States of America 99*, 13419-13424.

[3] Kuester, M., Becker, G. L., Hardes, K., Lindberg, I., Steinmetzer, T., and Than, M. E. (2011) Purification of the proprotein convertase furin by affinity chromatography based on PC-specific inhibitors, *Biological chemistry 392*, 973-981.

[4] Cameron, A., Appel, J., Houghten, R. A., and Lindberg, I. (2000) Polyarginines are potent furin inhibitors, *The Journal of biological chemistry 275*, 36741-36749.

[5] Dixon, M. (1953) The determination of enzyme inhibitor constants, *The Biochemical journal 55*, 170-171.

[6] Becker, G. L., Sielaff, F., Than, M. E., Lindberg, I., Routhier, S., Day, R., Lu, Y., Garten, W., and Steinmetzer, T. (2010) Potent inhibitors of furin and furin-like proprotein convertases containing decarboxylated P1 arginine mimetics, *Journal of medicinal chemistry 53*, 1067-1075.

[7] Williams, J. W., and Morrison, J. F. (1979) The kinetics of reversible tight-binding inhibition, *Methods in enzymology 63*, 437-467.

[8] Becker, G. L., Lu, Y., Hardes, K., Strehlow, B., Levesque, C., Lindberg, I., Sandvig, K., Bakowsky, U., Day, R., Garten, W., and Steinmetzer, T. (2012) Highly potent inhibitors of proprotein convertase furin as potential drugs for treatment of infectious diseases, *The Journal of biological chemistry 287*, 21992-22003.

[9] Mueller, U., Darowski, N., Fuchs, M. R., Forster, R., Hellmig, M., Paithankar, K. S., Puhringer, S., Steffien, M., Zocher, G., and Weiss, M. S. (2012) Facilities for macromolecular crystallography at the Helmholtz-Zentrum Berlin, *Journal of synchrotron radiation 19*, 442-449.

[10] Kabsch, W. (2010) Xds, *Acta crystallographica 66*, 125-132.

[11] Winn, M. D., Ballard, C. C., Cowtan, K. D., Dodson, E. J., Emsley, P., Evans, P. R., Keegan, R. M., Krissinel, E. B., Leslie, A. G., McCoy, A., McNicholas, S. J., Murshudov, G. N., Pannu, N. S., Potterton, E. A., Powell, H. R., Read, R. J., Vagin, A., and Wilson, K. S. (2011) Overview of the CCP4 suite and current developments, *Acta crystallographica 67*, 235-242.

[12] Kleywegt, G. J., and Jones, T. A. (1996) xdlMAPMAN and xdlDATAMAN - programs for reformatting, analysis and manipulation of biomacromolecular electron-density maps and reflection data sets, *Acta crystallographica 52*, 826-828.

[13] Henrich, S., Cameron, A., Bourenkov, G. P., Kiefersauer, R., Huber, R., Lindberg, I., Bode, W., and Than, M. E. (2003) The crystal structure of the proprotein processing proteinase furin explains its stringent specificity, *Nature structural biology 10*, 520-526.

[14] McCoy, A. J., Grosse-Kunstleve, R. W., Adams, P. D., Winn, M. D., Storoni, L. C., and Read, R. J. (2007) Phaser crystallographic software, *Journal of applied crystallography 40*, 658-674.

[15] Emsley, P., Lohkamp, B., Scott, W. G., and Cowtan, K. (2010) Features and development of Coot, *Acta crystallographica 66*, 486-501.

[16] Brunger, A. T. (2007) Version 1.2 of the Crystallography and NMR system, *Nature protocols 2*, 2728-2733.

[17] Allen, F. H. (2002) The Cambridge Structural Database: a quarter of a million crystal structures and rising, *Acta Crystallogr B 58*, 380-388.

[18] Kleywegt, G. J. (1997) Validation of protein models from Calpha coordinates alone, *Journal of molecular biology 273*, 371-376.

[19] Ericsson, U. B., Hallberg, B. M., Detitta, G. T., Dekker, N., and Nordlund, P. (2006) Thermofluor-based high-throughput stability optimization of proteins for structural studies, *Analytical biochemistry 357*, 289-298.
[20] Evans, P. (2006) Scaling and assessment of data quality, *Acta crystallographica 62*, 72-82.